Cent. Eur. J. Phys. • 9(6) • 2011 • 1493-1502
DOI: 10.2478/s11534-011-0070-z

VERSITA

Central European Journal of **Physics**

Merging of viral concentration waves in retrograde viral transport in axons

Research Article

Andrey V. Kuznetsov*

Dept. of Mechanical and Aerospace Engineering, North Carolina State University, Campus Box 7910, NC 27695-7910 Raleigh, USA

Received 23 May 2011; accepted 26 July 2011

Abstract: This paper develops an analytical solution describing propagation of two viral waves in an axon and applies the obtained analytical solution to investigating the dynamics of merging of these two waves as they move retrogradely toward the neuron body. The viral diffusivity and viral degradation are accounted for in the model. Computational results are presented for two situations: when all dynein motors move with the same velocity and when dynein motor velocity distribution is characterized by a probability density function (pdf). The effect of various model parameters on the time it takes for the waves to merge is discussed. It is proposed that observing the dynamics of wave merging can be used for determining parameters characterizing viral transport, such as the viral diffusivity. This may contribute toward better understanding of viral transport properties and potentially help in developing novel viral detection techniques.

PACS (2008): 87.16.-b

Keywords: neurotropic virus • retrograde axonal transport • molecular motors • virus trafficking

1. Introduction

Gene therapy that relies on delivery of special genes and various growth factors by using viral vectors, such as a modified adeno-associated viral (AAV) vector, demonstrated potential in retrograde delivery of the anti-apoptotic genes for neuronal protection [1], treating of spinal injury [2–4], glaucoma treatment [5], and promoting central nervous system repair [6].

Many neurotropic viruses (viruses that infect nerve cells) enter the axons at their presynaptic terminals [7]. Since viruses have no means to propel themselves independently, and since due to their size their diffusivity is small, after being internalized they have to rely on cellular transport machinery in order to reach the neuron soma [8].

The transport machinery of the cell is designed to move large organelles along microtubule (MT) tracks; the organelles are pulled by kinesin molecular motors in the anterograde direction (away from the cell body) and by dynein molecular motors in the retrograde direction (toward the cell body) [9–15]. Some viruses, such as the West Nile virus, can spread in both retrograde and anterograde directions [16]; however, most neurotropic viruses, such as the rabies virus, herpes virus, and polio virus enter the neuron via endocytosis at the presynaptic terminal of the axon and then utilize dynein motors in order to be trans-

*E-mail: avkuznet@ncsu.edu

ported in the retrograde direction toward the neuron soma [17–20].

Developing mechanistic understanding of viral transport in axons is important for finding ways of optimizing virus-based gene delivery vectors, developing novel treatments against harmful neurotropic viruses, and better understanding of intracellular transport in general. The latter is important for developing treatments for various neurodegenerative diseases since such diseases are usually related to abnormalities in intracellular trafficking [21, 22].

Better mechanistic understanding of virus transport is also important for creating novel techniques of virus detection. Standard viral detection methods, reviewed in Storch [23], relied on isolation and in vitro viral culture, direct fluorescence antibody, or enzyme immunoassay. Wang et al. [24] reported a DNA microarray-based viral detection technique with the potential to simultaneously detect hundreds of viruses. Recently, Daaboul et al. [25] reported an interferometric-based technique capable of detecting and size characterizing of various viruses, including H1N1 (flu) viruses.

When virus enters an axon, its concentration forms a wave that propagates toward the neuron soma. If such an entry occurred twice within a short period time (the situation when viral waves would enter a cell in a temporally coordinated fashion can be easily created in a lab), the two induced viral concentration waves will interact. The study of the interaction of such waves is physically interesting; the positions of the peaks of the waves can be used as markers in an experiment; this information can be useful for measuring certain parameters related to viral transport, such as the velocity of viral propagation, the rate of viral degradation and the viral diffusivity. A comparison of simulation results with a future experiment can provide insight into mechanisms of intracellular viral trafficking. The situation similar to that occurring in slow axonal transport has been studied numerically in [26, 27].

The purpose of this paper is to obtain an analytical solution describing retrograde viral transport in axons and demonstrate that this solution can be utilized to investigate a complicated situation involving interference and merging of two viral concentration waves. The solution method developed in this paper relies on mathematical techniques developed in [15, 28] for modeling retrograde transport of neurotropic viruses, in [29] for modeling the propagation of injury signals in axons, and in [30] for modeling retrograde transport of nerve growth factors.

2. Viral trafficking model

The model developed in this paper is based on equations governing active motor-assisted transport in cells developed in Smith and Simmons [31]; these equations were applied to various problems involving viral trafficking in [32–36]. However, unlike in the above papers, the model developed in the present research accounts for only one cargo population. This assumption is necessary to make an analytical solution possible. It is assumed that the virus (the cargo) can be transported by motor-driven transport (in that mode, it is most likely transported on MTs inside endosomes), but it can also experience diffusion-driven transport. Thus the model developed here accounts for both motor-driven and diffusion-driven viral transport, but does it using the framework of a single advection diffusion equation. It is expected that this simplification would result in some loss of resolution of the model, but it allows approaching the problem analytically. Another benefit is the absence of the kinetic terms describing transitions between various cargo populations. This is an important advantage since it is hard to estimate values of these kinetic constants from published experimental results (and it is probably hard to design an experiment to measure them). A schematic diagram of the problem is displayed in Fig. 1a. The virus enters the axon of a peripheral nervous system at the synapse (located at $x = 0$). It is assumed that the synapse is exposed to a constant viral flux, j_0, for a limited time, t_c, and then, after time t_d, to another viral pulse of the same intensity, also of duration t_c (the boundary condition at the synapse is illustrated in Fig. 1b). The viral diffusivity models transport of a free virus in the cytoplasm of the cell, as well as the situation when an endosome containing viral particles detaches from an MT. Diffusivity can also be caused by cargo navigation around obstacles during motor-driven transport. Degradation of the virus as it travels from the axon terminal toward the neuron soma is accounted for by a first-order decay rate (such degradation is important, for example, in the case of the poliovirus [17]). Under these assumptions, retrograde transport of viruses in an axon is governed by the following equation:

$$\frac{\partial n}{\partial t} = D\frac{\partial^2 n}{\partial x^2} - v_0\frac{\partial n}{\partial x} - kn, \qquad (1)$$

where D is the viral diffusivity, k is the kinetic constant describing the rate of viral degradation in the axon, n is the number density of viral particles, v_0 is the velocity of dynein motors, t is the time, and x is the linear coordinate directed from the presynaptic terminal to the axon hillock (see Fig. 1a). The total viral flux (by diffusion and motor-

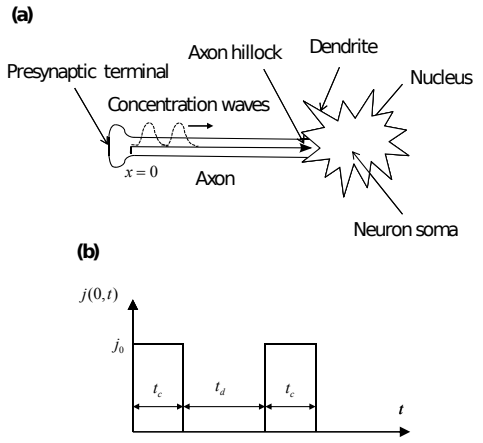

Figure 1. (a) Schematic diagram of the problem; (b) Viral flux at the axon terminal versus time (the boundary condition).

driven transport) is

$$j = -D\frac{\partial n}{\partial x} + v_0. \tag{2}$$

The boundary condition at x=0 is (see Fig. 1b):

$$j(0,t) = -D\frac{\partial n}{\partial x}(0,t) + v_0 n(0,t)$$

$$= j_0\{1 - H[t-t_c] + H[t-(t_d+t_c)] - H[t-(t_d+2t_c)]\}, \tag{3}$$

where $H[t]$ is the Heaviside step function.

It is assumed that the neuron soma acts as a perfect absorber of viruses (no wave reflection at the axon hillock, [37]), which means that the solution is identical to that obtained for a semi-infinite domain.

Eq. (1) with boundary condition (3) and zero initial condition (it is assumed that initially there are no viruses in the axon) is solved by Laplace transform. The subsidiary equation is

$$sN = D\frac{\partial^2 n}{\partial x^2} - v_0\frac{\partial N}{\partial x} - kN, \tag{4}$$

where $N(x,s)$ is the Laplace transform of the function $n(x,t)$.

The Laplace transform of boundary condition (3) is

$$-D\frac{\partial n}{\partial x}(0,s) + v_0\, N(0,s)$$

$$= j_0\frac{1 - e^{-st_c} + e^{-s(t_d+t_c)} - e^{-s(t_d+2t_c)}}{s}. \tag{5}$$

The solution of subsidiary Eq. (4) subject to boundary condition (5) and the condition that the solution remains finite as $x \to \infty$ is

$$N(x,s) = \frac{2j_0}{s(v_0 + \sqrt{v_0^2 + 4D(k+s)}}$$

$$\times\left\{\exp\left[\frac{v_0 - \sqrt{v_0^2 + 4D(k+s)}}{2D}x\right]\right.$$

$$-\exp\left[-st_c + \frac{v_0 - \sqrt{v_0^2 + 4D(k+s)}}{2D}x\right]$$

$$+\exp\left[-s(t_c+t_d) + \frac{v_0 - \sqrt{v_0^2 + 4D(k+s)}}{2D}x\right]$$

$$\left.-\exp\left[-s(2t_c+t_d) + \frac{v_0 - \sqrt{v_0^2 + 4D(k+s)}}{2D}x\right]\right\}. \tag{6}$$

The solution for the viral concentration is obtained by calculating the inverse Laplace transform [38] of the right-hand side of Eq. (6), the obtained solution is given by Eq. (A1) in the Appendix.

Eq. (A1) gives the viral concentration under the assumption that all dynein motors that propel retrograde viral transport move with the same velocity v_0 (in this equation v_0 is constant).

The following argument is utilized to approach the situation when the dynein velocity distribution is characterized by a pdf $f(v)$. Imagine that there are two species of viral particles, slow and fast. Slow particles move with velocity v_1 while fast particles move with velocity v_2. Assume that the flux of viral particles that enters the axon terminal consists by 20% of slow particles and by 80% of fast particles. One can say that $j_{0,slow} = 0.2j_0$ and $j_{0,fast} = 0.8j_0$, where j_0 is the total flux of particles at $x = 0$. Since according to Eq. (A1) the particle concentration is directly proportional to j_0, the concentration of slow particles in the axon is given by $0.2n(x,t;v_1)$ and the concentration of fast particles is given by $0.8n(x,t;v_2)$. The total concentration of viral particles is then given by $0.2n(x,t;v_1)+0.8n(x,t;v_2)$. This argument can now be extended to the infinite number of species of particles. It is assumed that velocities of particles entering the axon terminal are distributed according to $f(v)$. By using the superposition principle, one finds that the total concentration of particles is then given by the following integral:

$$n_{f(v)}(x,t) = \int_0^\infty n(x,t;v)\, f(v)dv. \tag{7}$$

It should be noted that although Eq. (1) is valid separately for each species of particles (with a corresponding velocity), the total concentration $n_{f(v)}$ defined by Eq. (7) does not satisfy Eq. (1). This is explained as follows. When considering the total concentration, one calculates the number of viral particles in a unit volume, all of them are moving with different velocities. The total concentration is thus found not by solving a fundamental conservation equation, but rather as a post-processing step, by taking a weighted average of the solutions of an infinite number of equations. In practice the integral on the right-hand side of Eq. (7) is calculated only over the interval of v where $f(v)$ is non-zero. If v is a constant (all dynein motors move with the same velocity v_0) then $f(v) = \delta(v - v_0)$ (where δ is a Dirac delta function) and the integral on the right-hand side of Eq. (7) collapses to $n(x, t; v_0)$.

3. Parameter estimation

In what follows order-of-magnitude estimates for different parameters involved in the model are presented. In [8, 39] the diffusivity of an AAV vector is estimated as 1.3 μm^2/s. In order to show the effect of diffusivity, computations are carried out for two values of D, 1 and 2 μm^2/s.

It is assumed that motor-driven retrograde viral transport is powered by dynein motors. Utilizing experimental data obtained in Ross et al. [40] and Deinhardt [41], Kam et al. [42] obtained two correlations for the distributions of dynein velocities based on these results. The results obtained in [42] are normalized so that $\int_0^\infty f(v)\delta v = 1$. This yields the following pdf of the dynein velocity distribution that is based on data reported in Ross et al. [40]:

$$f_1(v) = 5.8145\, v \exp\left[-\left(\frac{v - 0.2738}{0.3363}\right)^2\right]. \qquad (8)$$

The velocity of dynein motors in Eq. (8) must be given in μm/s (Eq. (8) is purely a curve-fit correlation); the function $f(v)$ has dimensions s/μm. Finding the expected value and the standard deviation of the dynein velocity from Eq. (8) results in $E(v) = 0.445$ μm/s and $\sigma(v) = 0.192$ μm/s, respectively.

The normalized pdf of the dynein velocity distribution that is based on data reported in Deinhardt et al. [41] is

$$f_2(v) = 1.4616\, v \exp\left[-\left(\frac{v + 0.6657}{1.7231}\right)^2\right]. \qquad (9)$$

In this case the expected value and the standard deviation of the dynein velocity are $E(v) = 1.272$ μm/s and $\sigma(v) = 0.504$ μm/s, respectively.

It is assumed that a single pulse contains 500 viral particles (1000 particles in two pulses). Since the problem is linear, this assumption does not affect the generality of the trends displayed in the figures. In order to estimate the flux of viral particles from the injury site, j_0 , one needs to know the duration of one viral pulse, t_c. Using, for example, a 60s duration of the pulse and estimating the average axonal diameter, d, as 1.1 μm based on [43] one obtains $j_0 = 8.8$ particles/(μm^2s). The time between the pulses, t_d, is assumed to be twice the pulse duration, 120s.

For plasmids, the disintegration rate was estimated as 1/3600 1/s [8, 44]. Two values are used for this parameter in the present research: $k = 0$ 1/s, which corresponds to the assumption that no degradation of the virus occurs, and $k = 10^{-3}$ 1/s, which corresponds to a relatively large rate of viral degradation.

4. Results and discussion

Fig. 2 displays viral concentration waves at three times: 300, 600, and 900 s. Fig. 2a is computed assuming that all dynein motors move with the same velocity ($v_1 = 0.445$ μm/s) and Fig. 2b is computed assuming that there is a distribution of dynein velocities, which is based on data reported in Ross et al. [40] (v_1 used for Fig. 2a is obtained as an expected value of this velocity distribution). Other parameter values utilized for this figure are $D = 1$ μm^2, $j_0 = 8.8$ 1/μm^2s, $t_c = 60$ s, $t_d = 120$ s and $k = 0$ 1/s. The solution given by Eq. (A1) approaches a finite limit as $k \to 0$; to obtain this limit numerically the value of k was reduced until the result became independent of k. In Fig. 2a one can see how two waves merge (the merging is complete by approximately $t = 900$ s). It should be noted that merging of the waves is observed only if dynein velocity is assumed constant; in Fig. 2b, which is computed for the case when dynein velocity is distributed, the two pulses do not induce two distinct waves, which is due to a broad range of dynein velocities, so the waves merge right at the beginning. Observing this situation in a future experiment can thus suggest how nonuniform the dynein velocity distribution is in a particular cellular system.

Fig. 3 is similar to Fig. 2, but it is computed for the dynein motor velocity distribution based on Deinhardt et al. [41] data. This distribution gives a much larger expected motor velocity ($v_2 = 1.272$ μm/s, which is 2.86 times larger than the value used for Fig. 2a). Since the waves in Fig. 3a merge much slower than those displayed in Fig. 2a, the waves are shown at larger times, 2000, 4000, and 6000 s. To explain why the time when the waves merge is affected

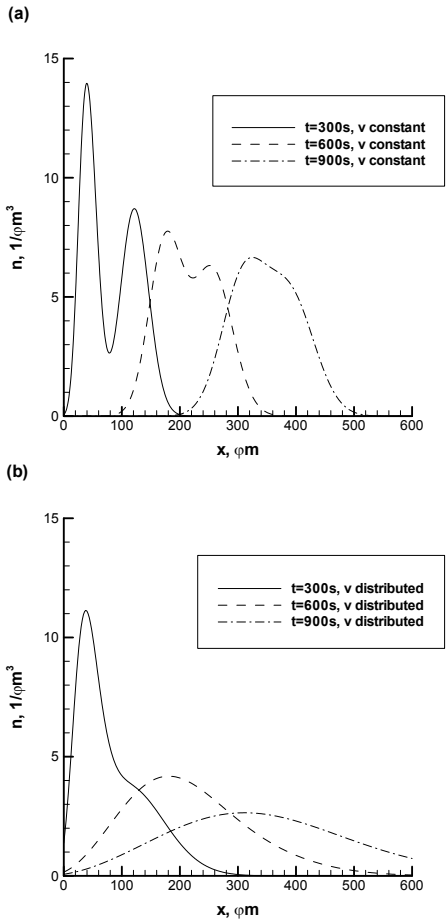

Figure 2. Viral concentration waves at various times. (a) Constant velocity of all dynein motors is assumed (calculated as an expected value of a corresponding velocity distribution); (b) A pdf describing the dynein motor velocity distribution based on Ross et al. [40] data is assumed. ($D = 1\ \mu\text{m}^2/\text{s}$, $j_0 = 8.8\ 1/\mu\text{m}^2\text{s}$, $t_c = 60$ s, $t_d = 120$ s, $k = 0$ 1/s).

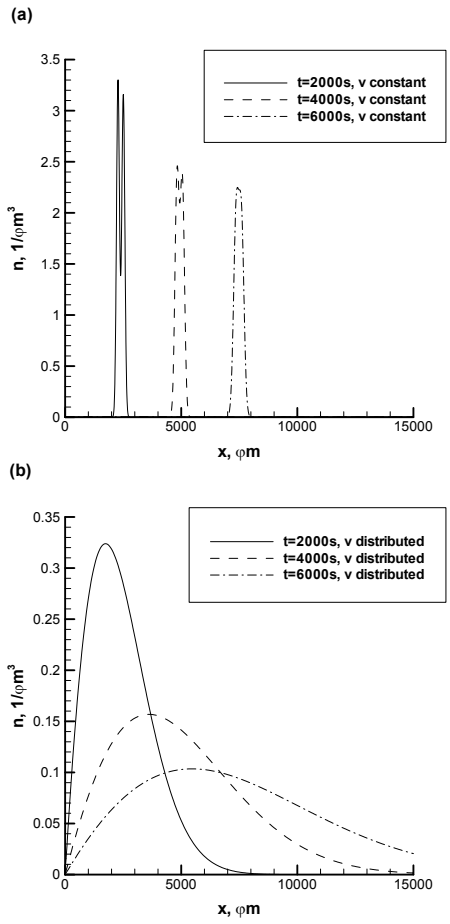

Figure 3. Similar to Fig. 2, but now for the dynein motor velocity distribution based on Deinhardt et al. [41] data.

to such a degree by the motor velocity, Eq. (1) is converted into its dimensionless form:

$$\frac{\partial \hat{n}}{\partial \hat{t}} = \hat{D}\frac{\partial^2 \hat{n}}{\partial \hat{x}^2} - \frac{\partial \hat{n}}{\partial \hat{x}} - \hat{n}, \tag{10}$$

where the dimensionless variables are defined as follows:

$$\hat{D} = \frac{Dk}{v^2}, \quad \hat{x} = \frac{xk}{v}, \quad \hat{n} = n\frac{v}{j_0}, \quad \hat{t} = tk. \tag{11}$$

One can check that if one recomputes the results utilizing the same dynein velocity that was used for Fig. 3a ($v_2 = 1.272\ \mu$m/s) but modifies the rest of the parameters as follows

$$D^* \to \left(\frac{v_2}{v_1}\right)^2 D,\ n^* \to \frac{v_2}{v_1}n,\ x^* \to x/\left(\frac{v_2}{v_1}\right), \tag{12}$$

and uses $t = 300, 600$, and 900 s, one obtains the results displayed in Fig. 2a. This means that the results for a smaller velocity v_1 can be recovered from the results for a larger velocity v_2 by increasing diffusivity by a factor of $\left(\frac{v_2}{v_1}\right)^2$, increasing the wave amplitude by a factor of $\frac{v_2}{v_1}$, and shrinking x by a factor of $\frac{v_2}{v_1}$.

Figs. 4 and 5 are similar to Figs. 2 and 3, but they are computed for a non-zero rate of viral degradation, $k = 10^{-3}$ 1/s. Figs. 4a and 4b are quite similar to Figs. 2a and 2b, in the former figures one can see a small decrease of the amplitude of the waves due to viral degradation. The difference between Figs. 5a and 5b and Figs. 3a and 3b is much larger (the decrease of the wave's amplitude due to viral degradation is much more pronounced), and this is because of larger times used in computing Figs. 3 and 5 than those used in computing Figs. 2 and 4. The effect of viral degradation is thus important for large times

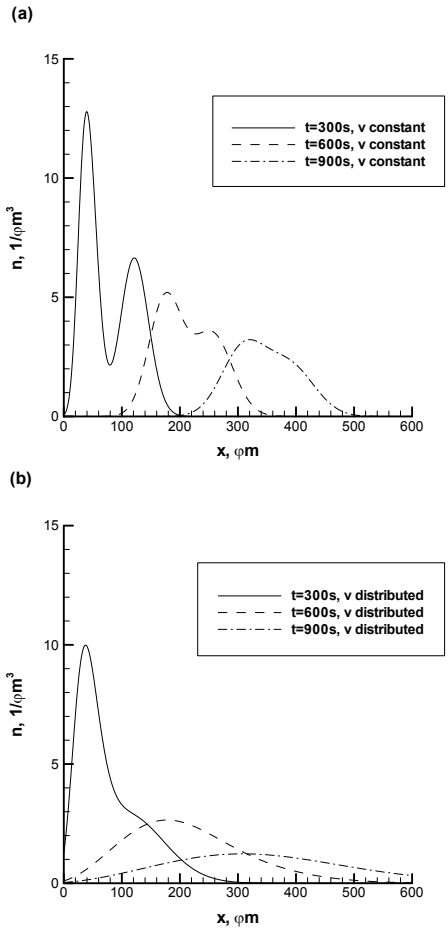

Figure 4. Similar to Fig. 2, but now for non-zero rate of viral degradation, $k = 10^{-3}$ 1/s.

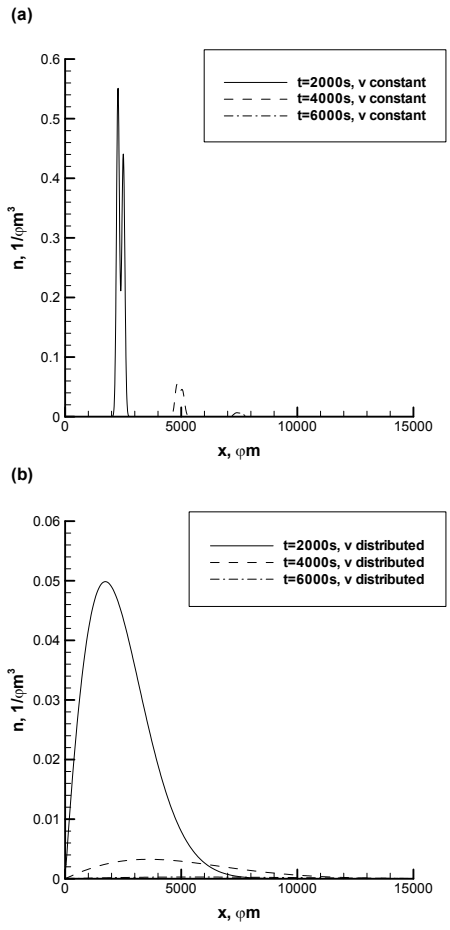

Figure 5. Similar to Fig. 3, but now for non-zero rate of viral degradation, $k = 10^{-3}$ 1/s.

and not so important for small times. This is because this is a cumulative effect that takes time to become significant.

Fig. 6 is similar to Fig. 2, but it is computed for twice larger viral diffusivity, $D = 2\ \mu m^2/s$. A comparison between Fig. 6a and Fig 2a shows that the increased diffusivity results in merging of the waves at a much earlier time (by $t = 600$ s the waves in Fig. 6a have completely merged). This suggests that by observing the shape of the wave and the dynamics of the waves' peaks in an experiment it is possible to make conclusions about the viral diffusivity. When two different types of viruses have different diffusivities, one can envision developing a test based on observing the dynamics and interference of the two waves. The difference between Figs. 6b and 2b is much less than that between Figs. 6a and 2a, which is explained by the fact that the dynein velocity distribution smoothens concentration gradients, which results in less sensitivity to the viral diffusivity.

Fig. 7 is similar to Fig. 3, but it is computed for a twice larger diffusivity, $D = 2\ \mu m^2/s$. The trends that can be deduced from comparing these two figures are similar to those that follow from comparing Figs. 6 and 2. The amplitudes of the waves in Fig. 7a decay faster than in Fig. 3a and the waves merge faster as well. There is much less difference between Figs. 7b and 3b due to the smoothing effect of the dynein velocity distribution.

Fig. 8 displays values of x where the function $n(x)$ takes its maximum values. In physical terms, Fig. 8 shows positions of the two peaks of the concentration waves. Constant velocity of dynein motors is assumed. Fig. 8a is computed using the expected value of dynein velocity that follows from Ross et al. [40] data ($v_1 = 0.445\ \mu m/s$) and Fig. 8b is computed using the expected value of dynein velocity that follows from Deinhardt et al. [41] data ($v_2 = 1.272\ \mu m/s$). Fig. 8 is computed for the case

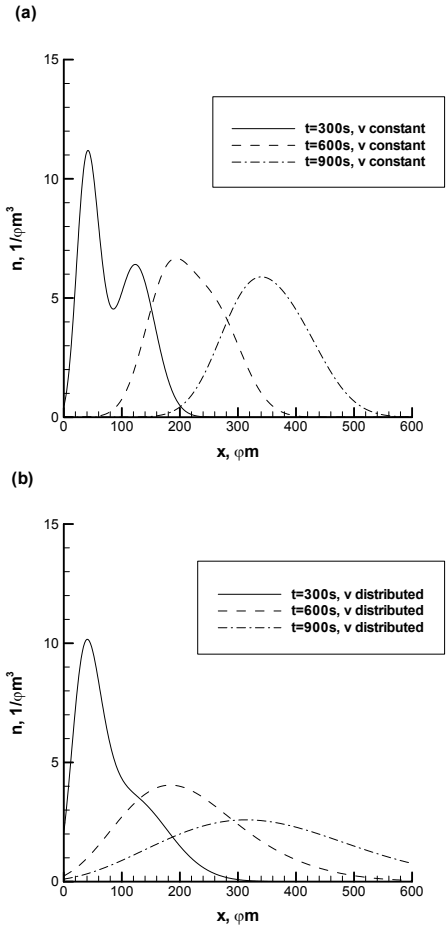

Figure 6. Similar to Fig. 2, but now for a twice larger value of diffusivity, $D = 2\,\mu\text{m}^2/\text{s}$.

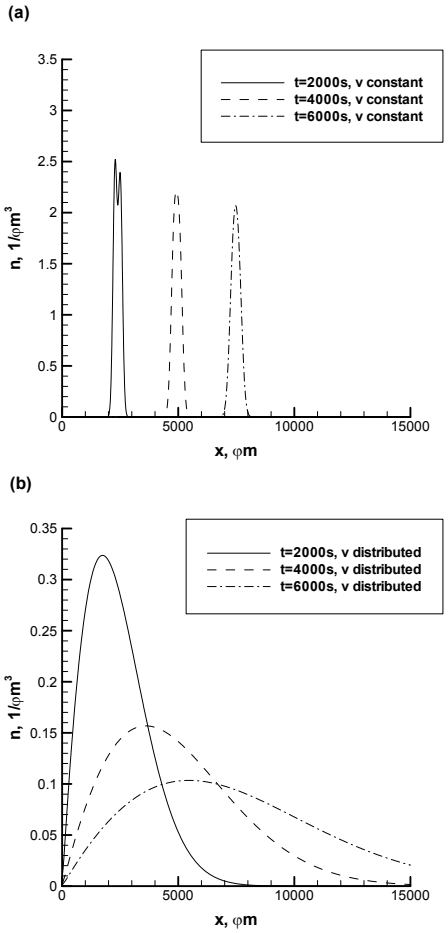

Figure 7. Similar to Fig. 3, but now for a twice larger value of diffusivity, $D = 2\,\mu\text{m}^2/\text{s}$.

with no viral degradation, $k = 0$ 1/s. Fig. 8a thus corresponds to the waves displayed in Fig. 2a (in this case the waves merge at $t_m = 732$ s) and Fig. 8b corresponds to those displayed in Fig. 3a (in this case the waves merge at $t_m = 5978$ s). As long as the waves are distinct, there are two peaks. Eventually, the first peak disappears (see Fig. 8a), and from that moment on one can say that the two waves have merged. It is evident that as the waves propagate, the two peaks become closer, but only slightly, so merging of the two waves is not a process involving the coalescence of two peaks; rather, the first peak becomes less and less pronounced and eventually becomes a region with a horizontal slope.

Fig. 9 is similar to Fig. 8, but it is computed for $k = 10^{-3}$ 1/s. It is evident that as a result of increased k the waves merge a little faster. In Fig. 9a merging occurs at $t_m = 666$ s, 9.0% earlier than in Fig. 8a, and in Fig. 9b merging occurs at $t_m = 4902$ s, 18.0% earlier than in Fig. 8b. Fig. 10 is similar to Fig. 8, but it is computed for $D = 2\,\mu\text{m}^2/\text{s}$. This means that Fig. 8a corresponds to the waves displayed in Fig. 6a and Fig. 8b corresponds to those displayed in Fig. 7a. By comparing Figs. 10a,b with Figs. 8a,b one can see that the first peak disappears at much smaller time, which means that the increase of D results in the waves merging much earlier. In Fig. 10a merging occurs at $t_m = 422$ s, 42.3.0% earlier than in Fig. 8a, and in Fig. 10b merging occurs at $t_m = 2931$ s, 51.0% earlier than in Fig. 8b.

5. Conclusions

Two waves of viral concentration are induced in the axon by subjecting the presynaptic terminal to two impulses, each of duration of 60 s, of a constant viral flux, with 120 s between the impulses. Two cases are simulated:

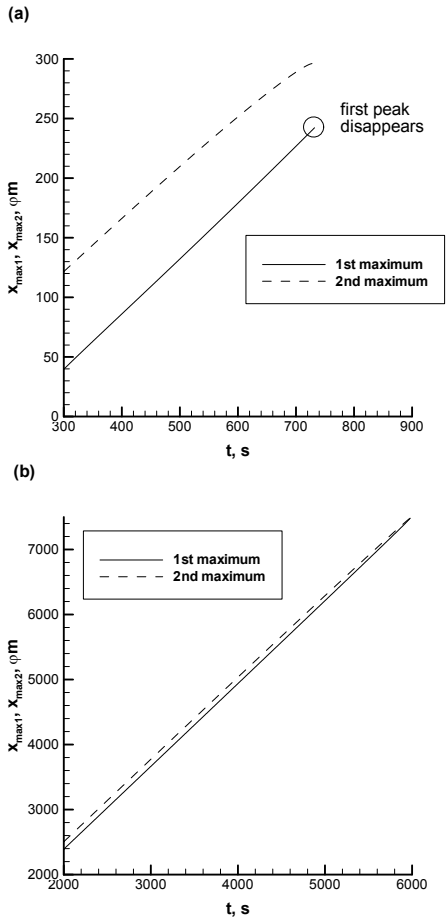

Figure 8. Positions of the waves' peaks versus time computed for the case when all dynein motors move with the same velocity. (a) The dynein velocity equals to the expected value that follows from Ross et al. [40] data (0.4453 μm/s); (b) The dynein velocity equals to the expected value that follows from Deinhardt et al. [41] data (1.272 μm/s). ($D = 1\mu m^2/s$, $j_0 = 8.8\,1/\mu m^2 s$, $t_c = 60$ s, $t_d = 120$ s, $k = 0$ 1/s).

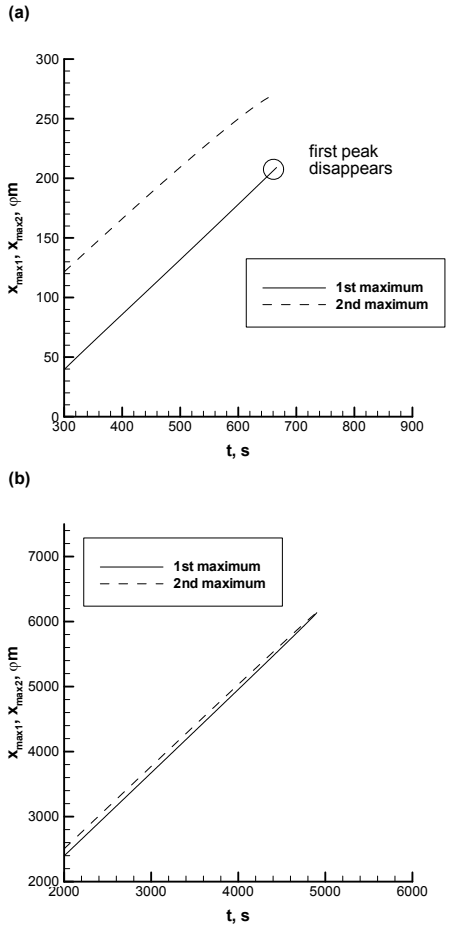

Figure 9. Similar to Fig. 8, but now for $k = 10^{-3}$ 1/s.

when all dynein motors move with the same velocity and when there is a distribution of dynein motor velocities. Merging of the waves is observed only if dynein velocity is assumed constant; when dynein velocity is distributed, the two pulses do not induce two distinct waves, the concentration disturbances in this case merge right in the beginning.

For the case when the dynein velocity is constant, the increase of the rate of viral degradation results in a faster decay of the amplitude of the wave and slightly decreases the time that it takes for the waves to merge. Increasing a value of k from 0 (no viral degradation) to 10^{-3} 1/s (large rate of viral degradation) reduces the time it takes for the waves to merge by 9 to 18%, depending on the velocity of dynein motors. The increase of the viral diffusivity has a much stronger effect on the rate of waves' merging. Increasing the value of D from 1 to 2 $\mu m^2/s$ reduces the time that it takes for the waves to merge by 42 to 51%, depending on the dynein velocity.

The obtained results suggest that when two types of viruses have different transport parameters, for example, different diffusivity, observing the dynamics of merging of two viral waves can provide reliable insights for developing novel virus detection techniques.

Appendix A

Calculating the inverse Laplace transform [38] of the right-hand side of Eq. (6), the following solution for the case when all dynein motors move with the same velocity

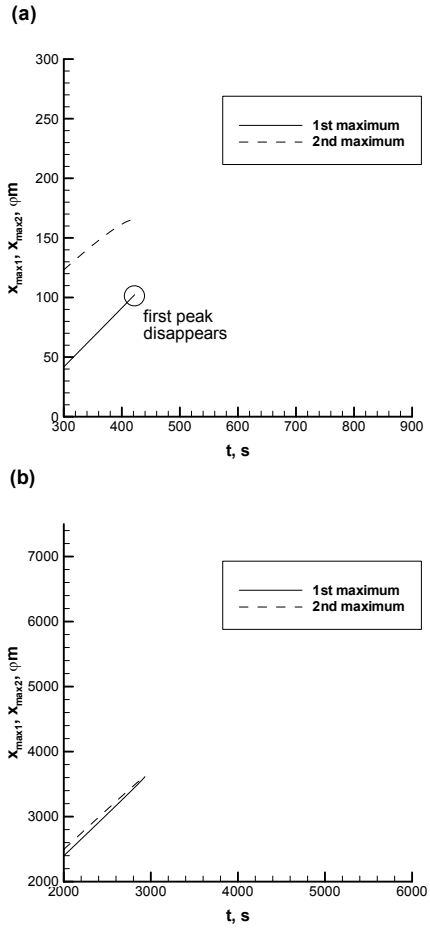

Figure 10. Similar to Fig. 8, but now for $D = 2\,\mu m^2/s$.

v_0 is obtained:

$$n(x,t;v_0) = \frac{j_0}{4Dk}\exp\left[\frac{\left(v_0-\sqrt{4Dk+v_0^2}\right)x}{2D}\right]$$

$$\times\left\{\exp[-kt]\left[2\exp\left[\frac{\left(v_0+\sqrt{4Dk+v_0^2}\right)x}{2D}\right]\right.\right.$$

$$\left.\times\, v_0\,\mathrm{erfc}\left[\frac{tv_0+x}{2\sqrt{Dt}}\right]\right.$$

$$+e^{kt}\left\{\left(-v_0+\sqrt{4Dk+v_0^2}\right)\mathrm{erfc}\left[\frac{-t\sqrt{4Dk+v_0^2}+x}{2\sqrt{Dt}}\right]\right.$$

$$-\exp\left[\frac{x\sqrt{4Dk+v_0^2}}{D}\right]\left(v_0+\sqrt{4Dk+v_0^2}\right)$$

$$\times\,\mathrm{erfc}\left[\frac{t\sqrt{4Dk+v_0^2}+x}{2\sqrt{Dt}}\right]\Bigg\}\Bigg]+\Bigg\{-2\,exp\,[k(-t+t_c)$$

$$+\frac{\left(v_0+\sqrt{4Dk+v_0^2}\right)x}{2D}\Bigg]v_0\,\mathrm{erfc}\left[\frac{tv_0-t_cv_0+x}{2\sqrt{D(t-t_c)}}\right]$$

$$+\exp\left[\frac{x\sqrt{4Dk+v_0^2}}{D}\right]\left(v_0+\sqrt{4Dk+v_0^2}\right)$$

$$\times\,\mathrm{erfc}\left[\frac{(t-t_c)\sqrt{4Dk+v_0^2}+x}{2\sqrt{D(t-t_c)}}\right]+\left(v_0-\sqrt{4Dk+v_0^2}\right)$$

$$\times\,\mathrm{erfc}\left[\frac{(-t+t_c)\sqrt{4Dk+v_0^2}+x}{2\sqrt{D(t-t_c)}}\right]\Bigg\}\,H(t-t_c)$$

$$+\Bigg\{-2\exp\left[k(-t+2t_c+t_d)+\frac{\left(v_0+\sqrt{4Dk+v_0^2}\right)x}{2D}\right]$$

$$\times\,v_0\,\mathrm{erfc}\left[\frac{tv_0-(2t_c+t_d)v_0+x}{2\sqrt{D(t-2t_c-t_d)}}\right]+\exp\left[\frac{x\sqrt{4Dk+v_0^2}}{D}\right]$$

$$\times\left(v_0+\sqrt{4Dk+v_0^2}\right)\mathrm{erfc}\left[\frac{(t-2t_c-t_d)\sqrt{4Dk+v_0^2}+x}{2\sqrt{D(t-2t_c-t_d)}}\right]$$

$$+\left(v_0-\sqrt{4Dk+v_0^2}\right)$$

$$\times\,\mathrm{ercf}\left[\frac{(-t+2t_c+t_d)\sqrt{4Dk+v_0^2}+x}{2\sqrt{D(t-2t_c-t_d)}}\right]\Bigg\}\,H(t-2t_c-t_d)$$

$$+\Bigg\{2\exp\left[k(-t+t_c+t_d)+\frac{\left(v_0+\sqrt{4Dk+v_0^2}\right)x}{2D}\right]$$

$$\times\,v_0\,\mathrm{erfc}\left[\frac{tv_0-(t_c+t_d)v_0+x}{2\sqrt{D(t-t_c-t_d)}}\right]-\exp\left[\frac{x\sqrt{4Dk+v_0^2}}{D}\right]$$

$$\times\left(v_0+\sqrt{4Dk+v_0^2}\right)\mathrm{erfc}\left[\frac{(t-t_c-t_d)\sqrt{4Dk+v_0^2}+x}{2\sqrt{D(t-t_c-t_d)}}\right]$$

$$+\left(-v_0+\sqrt{4Dk+v_0^2}\right)$$

$$\times\,\mathrm{erfc}\left[\frac{(-t+t_c+t_d)\sqrt{4Dk+v_0^2}+x}{2\sqrt{D(t-t_c-t_d)}}\right]\Bigg\}\,H(t-t_c-t_d)\Bigg\}, \tag{A1}$$

where erfc (τ) is the complementary error function. It should be noted that the right-hand side of Eq. (1) approaches a finite limit when $k \to 0$.

References

[1] B. K. Kaspar et al., Mol. Ther. 5, 50 (2002)
[2] Y. Liu et al., Brain Res. 768, 19 (1997)
[3] D. D. Pearse, M. B. Bunge, J. Neurotraum. 23, 438 (2006)
[4] X. N. Bo, D. S. Wu, J. Yeh, Y. Zhang, Curr. Gene. Ther. 11, 101 (2011)
[5] K. R. G. Martin et al., Invest. Ophth. Vis. Sci. 44, 4357 (2003)
[6] M. Berry et al., Curr. Opin. Mol. Ther. 3, 338 (2001)
[7] E. L. Bearer et al., Biol. Bull. 197, 257 (1999)
[8] T. Lagache, E. Dauty, D. Holcman, Curr. Opin. Microbiol. 12, 439 (2009)
[9] L. S. B. Goldstein, Z. H. Yang, Annu. Rev. Neurosci. 23, 39 (2000)
[10] S. P. Gross, Phys. Biol. 1, R1 (2004)
[11] M. A. Welte, Curr. Biol. 14, R525 (2004)
[12] P. E. Gallant, J. Neurocytol. 29, 779 (2000)
[13] A. D. Pilling, D. Horiuchi, C. M. Lively, W. M. Saxton, Mol. Biol. Cell. 17, 2057 (2006)
[14] S. Ally et al., J. Cell. Biol. 187, 1071 (2009)
[15] A. V. Kuznetsov, Cent. Eur. J. Phys. 9, 1372 (2011)
[16] M. A. Samuel et al., P. Natl. Acad. Sci. USA. 104, 17140 (2007)
[17] K. Z. Lancaster, J. K. Pfeiffer, Plos. Pathog. 6, e1000791 (2010)
[18] N. D. Mazarakis et al., Hum. Mol. Genet. 10, 2109 (2001)
[19] M. Miranda-Saksena et al., J. Virol. 83, 3187 (2009)
[20] G. S. Tan, M. A. R. Preuss, J. C. Williams, M. J. Schnell, P. Natl. Acad. Sci. USA. 104, 7229 (2007)
[21] S. Gunawardena, L. S. B. Goldstein, J. Neurobiol. 58, 258 (2004)
[22] E. L. F. Holzbaur, Res. Per. Alz. 27 (2009)
[23] G. A. Storch, Essentials of Diagnostic Virology (Churchill Livingstone, New York, 2000)
[24] D. Wang et al., P. Natl. Acad. Sci. USA. 99, 15687 (2002)
[25] G. G. Daaboul et al., Nano. Lett. 10, 4727 (2010)
[26] A. V. Kuznetsov, A. A. Avramenko, D. G. Blinov, Cent. Eur. J. Phys. 9, 898 (2011)
[27] A. V. Kuznetsov, A. A. Avramenko, D. G. Blinov, Int. J. Numer. Meth. Biomed. Engng. 27, 1040 (2011)
[28] A. V. Kuznetsov, Int. Commun. Heat. Mass. (in press)
[29] A. V. Kuznetsov, Comput. Method. Biomec. (submitted)
[30] A. V. Kuznetsov, Comput. Method. Biomec. (in press, DOI:10.1080/10255842.2011.607445)
[31] D. A. Smith, R. M. Simmons, Biophys. J. 80, 45 (2001)
[32] A. T. Dinh, T. Theofanous, S. Mitragotri, Biophys. J. 89, 1574 (2005)
[33] A. Dinh, C. Pangarkar, T. Theofanous, S. Mitragotri, Biophys. J. 92, 831 (2007)
[34] A. V. Kuznetsov, A. A. Avramenko, Int. Commun. Heat. Mass. 35, 395 (2008)
[35] A. V. Kuznetsov, A. A. Avramenko, Cent. Eur. J. Phys. 6, 45 (2008)
[36] A. V. Kuznetsov, A. A. Avramenko, D. G. Blinov, Comput. Method. Biomec. 11, 215 (2008)
[37] B. Engquist, A. Majda, Math. Comput. 31, 629 (1977)
[38] H. S. Carslaw, J. C. Jaeger, Conduction of heat in solids, 2nd (Clarendon Press, Oxford, 1959)
[39] G. Seisenberger et al., Science 294, 1929 (2001)
[40] J. L. Ross et al., Nature. Cell. Biology 8, 562 (2006)
[41] K. Deinhardt et al., Neuron, 52, 293 (2006)
[42] N. Kam, Y. Pilpel, M. Fainzilber, Plos. Comput. Biol. 5, e1000477 (2009)
[43] E. Bergers et al., Neurology 59, 1766 (2002)
[44] D. Lechardeur et al., Gene. Ther. 6, 482 (1999)